

Topological electrider phase of sodium at high pressures and temperaturesBusheng Wang ¹, Katerina P. Hilleke ¹, Xiaoyu Wang,¹ Danae N. Polsin,^{2,3} and Eva Zurek ^{1,4,5,*}¹*Department of Chemistry, State University of New York at Buffalo, Buffalo, New York 14260-3000, USA*²*University of Rochester Laboratory for Laser Energetics, Rochester, New York 14623, USA*³*Department of Mechanical Engineering, University of Rochester, Rochester, New York 14627, USA*⁴*Department of Physics, State University of New York at Buffalo, Buffalo, New York 14260-3000, USA*⁵*Department of Chemical and Biological Engineering, State University of New York at Buffalo, Buffalo, New York 14260-3000, USA*

(Received 12 May 2022; revised 20 April 2023; accepted 24 April 2023; published 3 May 2023)

Sodium, a textbook example of a nearly-free-electron metal, exhibits unforeseen pressure-induced behavior including the stabilization of numerous polymorphs—some possessing extremely complex unit cells—as well as a metal-to-insulator transition to the iconic *hP4* phase. However, until recently, most of the experimental and theoretical studies on solid sodium have been restricted to the low-temperature regime. Herein, using *ab initio* evolutionary structure searches coupled with quasiharmonic calculations, we discover seven new phases of sodium that are more stable than the known *hP4* phase at pressure-temperature conditions that were recently attained in ramp-compression experiments. From these, our calculations suggest that $P6_3/m$ Na is the ground state between ≈ 250 GPa at 710 K and ≈ 350 GPa at 1900 K. Electronic structure calculations show that this phase is a topological semimetal with a Dirac nodal surface that is protected by a nonsymmorphic symmetry S_{2z} and an electrider owing to its non-nuclear charge localized within one-dimensional honeycomb channels and zero-dimensional cages. Our results highlight the complexity of dense sodium's free-energy landscape and intricate electronic structure that emerges at finite temperatures and conditions where ionic cores overlap.

DOI: [10.1103/PhysRevB.107.184101](https://doi.org/10.1103/PhysRevB.107.184101)**I. INTRODUCTION**

Since the dawn of quantum mechanics, it has been assumed that, at sufficiently high pressures, all matter would adopt simple structures with densely packed ionic cores and nearly free electrons. However, unprecedented structural complexity and anomalous physical properties have been theoretically predicted and observed in the phase diagrams of the alkali metals [1]. In sodium, unexpected behavior is found already at ambient pressure where the bcc structure undergoes a partial martensitic phase transition upon cooling [2]. Compression to ≈ 120 GPa results in an astounding ≈ 700 K decrease in the melting point [3], whose minimum is associated with rich structural diversity [4,5]. Near 200 GPa and room temperature a transition to an insulating *hP4* phase occurs [6], and this phase persists upon ramp compression to nearly 500 GPa [7].

This extraordinary behavior of Na was foreseen by Neaton and Ashcroft who postulated that at pressures large enough to induce $2p$ orbital overlap, sodium's valence electrons would be impelled into the interstitial regions of its crystal lattice due to orthogonality and Pauli repulsion, resulting in a metal-to-insulator transition [8]. About a decade later this prediction was verified in static compression experiments that reported a double hexagonal *hP4* structure ($P6_3/mmc$, No. 194) with a band-gap exceeding 1.3 eV [6]. The *hP4* phase is characterized by electrons that are localized at lattice

voids—rendering it a prototypical example of a high-pressure electrider, where the ionic cores play the role of cations, and interstitial electrons act as anions. Such non-nuclear electron localization upon densification has been explained by core exclusion and proximity [9], *p-d* hybridization [6], and by comparing the pressure dependence of orbitals centered on interstitial quasiatoms to those centered on ionic cores [10,11]. Density-functional theory (DFT) calculations have shown that sodium's unusual optical properties [12], melting behavior, and rich polymorphism are consequences of the electrider state [13]. First-principles molecular-dynamics simulations find that localized electron bubbles persist in the fluid at high temperatures and pressures [14,15].

Moving to denser structures yet, cold DFT calculations predict that Na will transition from an insulating *oP8* phase to a metallic *cI24* phase characterized by Na_{12} icosahedra near 15.5 TPa [16]. Comparison of the Gibbs free energies of these phases obtained within the quasiharmonic approximation at 20 TPa and 1000 K led to the conclusion that the effect of temperature on the phase transition pressure is negligible. In contrast, laser-driven ramp-compression experiments of Na to nearly 500 GPa and ≈ 3000 K hint of temperature-dependent structural complexity at these conditions [7]. Specifically, *in situ* x-ray diffraction (XRD) revealed a series of phases upon recrystallization, with peaks attributed to Na *hP4* evident only above 400 GPa. At lower pressures (≈ 240 – 325 GPa) the obtained diffraction peaks could not be explained by the *hP4* structure, and other candidates were proposed. Herein, we aim to study the effect of finite temperature on phase stability in this pressure regime.

*ezurek@buffalo.edu

Topological quantum materials have been intensely studied over the last two decades and most of the known inorganic materials—primarily those stable at ambient pressure and temperature conditions—have been categorized according to their topological properties [17,18]. However, most of the matter in the Universe is found at pressures and temperatures so extreme that exotic crystal structures are assumed, core electrons interact, and atomic-orbital energies are reordered—sometimes promoting the occupation of non-atom-centered orbitals [11]. All of these factors can affect the electronic structure of matter, and theoretical studies have predicted various topological Group I elements and their alloys under pressure. For example, DFT calculations have shown that forms of dense hydrogen [19] and Na *hP4* [20] possess metallic surface states, the band structure of Li₅H presents Dirac-like features [21], and various phases of Li at intermediate pressures were computed to be topological semimetals with nodal loops or lines in the vicinity of the Fermi level, E_F [22,23]. The interest in topological semimetals stems from their unique properties including high mobilities [24], giant magnetoresistance [25], and because their massless fermions make it possible to simulate intriguing high-energy and relativistic physics phenomena in table-top experiments [26]. Topological semimetals may be characterized by the presence of zero-dimensional (0D) point nodes, one-dimensional (1D) nodal lines, or two-dimensional (2D) nodal surfaces where the conduction and valence bands cross in the Brillouin zone (BZ) [27].

This work presents a theoretical investigation of the structural complexity, topological features and core-electron chemistry emerging in sodium in a pressure and temperature regime that is near the core conditions of Earth-like planets and mantles of superearths. Using evolutionary algorithm searches coupled with first principles calculations, we predict several structures whose free energies fall below that of Na *hP4* above 200 GPa at finite temperatures, highlighting the potential for polymorphism within dense sodium at temperatures below the melting curve. A $P6_3/m$ Na phase is demonstrated to possess the lowest free energy between 250 GPa at 710 K, and 350 GPa at 1900 K. DFT calculations show that its electron density is localized within honeycomb channels and at interstitial sites, rendering it a semimetallic electride, with a Dirac nodal surface that is topologically protected by the nonsymmorphic symmetry S_{2z} . Therefore, tuning the P - T conditions in sodium provides another way to access topological materials. Our computations illustrate previously unexplored polymorphism and structural complexity just below the melting line of dense sodium and reveal that core-electron chemistry under extreme conditions of pressure and temperature can result in the emergence of novel topological phases of matter.

II. METHODS

Crystal structure prediction searches were carried out using the in-house developed XTALOPT [28,29] evolutionary algorithm release 12 [30], which was designed to find stable and metastable structures given only their composition. The geometry optimizations and electronic structure calculations were performed using the Vienna *ab initio* simulation

package (VASP) [31,32] coupled with the Perdew-Burke-Ernzerhof (PBE) gradient-corrected exchange and correlation functional [33]. The electron-ion interaction was described by the projector-augmented-wave method with the Na $2p^6 3s^1$ configuration treated as valence. We employed a kinetic-energy cutoff of 1000 eV and a Γ -centered Monkhorst-Pack scheme [34] where the number of divisions along each reciprocal-lattice vector was chosen such that its product with the real lattice constant was 50 Å. The phonon band structures were calculated using the supercell approach and/or density functional perturbation theory (DFPT) [35,36] with the VASP and PHONOPY [37] codes. Helmholtz free-energy data at finite temperature conditions, including the electron thermal and vibrational contributions, were calculated under the quasiharmonic approximation implemented in the PHONOPY-QHA script. Moreover, *ab initio* molecular dynamics (AIMD) simulations were performed within the canonical (NVT) ensemble to evaluate the thermal stability of specific phases up to 2000 K. A Nosé-Hoover thermostat was employed with a 2 fs time step and a total simulation time of 10 ps. The finite-temperature renormalized phonon spectra were calculated using phonon mode decomposition and AIMDs' projection technique, which was implemented in the DYNAPHOPY package [38]. To study the topological edge states, a first-principles tight-binding model Hamiltonian was constructed using the hopping parameters obtained from Wannier functions calculated with the VASP2WANNIER90 interface [39]. The Na s and p orbitals were used to build the maximally localized Wannier functions. The edge states were calculated using the iterative Green's function method as implemented in the WANNIERTOOLS package [40]. The topological properties of the sodium phases were obtained using the SYMTOPO package [41], which calculates the compatibility conditions of the band representations along high-symmetry lines in the BZ. Additional computational details are provided in the Supplemental Material [42].

III. RESULTS

In this paper we report seven theoretically predicted (meta)stable phases of sodium whose free energies fall within 40–90 meV/atom of each other in a temperature and pressure range where recent experiments suggest a rich structural polymorphism (≈ 300 GPa and ≈ 2000 K) [7]. Although the XRD patterns obtained in these experiments at the highest pressures were consistent with the well-known insulating *hP4* phase, the peaks observed at intermediate pressures could not be explained by this structure. Instead, between 242–292 GPa the patterns were attributed to a $cI16$ phase, isostructural with known phases of Li and Na found at lower temperatures and pressures, and at 315 GPa to a $R\bar{3}m$ symmetry structure. However, due to a limited number of observed diffraction peaks, the true structure solution may be even more complex than these. Indeed, our calculated phonon band structures and molecular-dynamics trajectories showed that the proposed $cI16$ and $R\bar{3}m$ structures are dynamically unstable at 260 and 315 GPa, respectively, and thermally unstable at these pressures and temperatures of 1500 and 2000 K, respectively (see Sec. S6 of the Supplemental Material [42]).

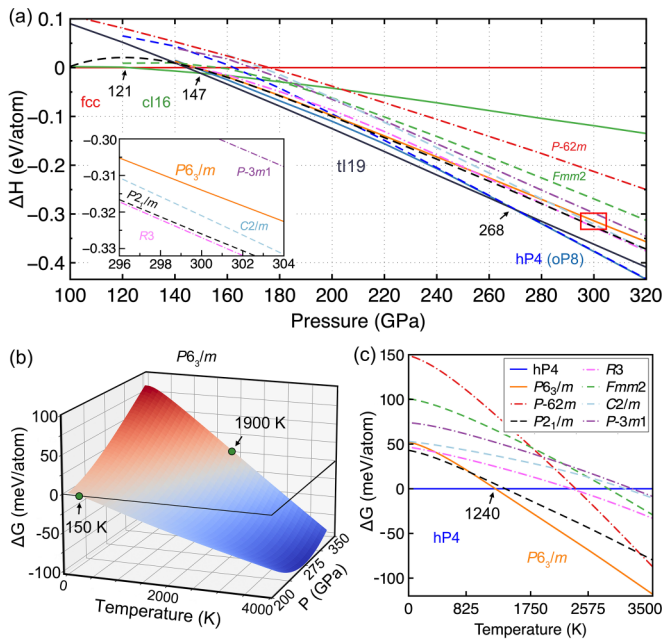


FIG. 1. (a) Enthalpies of various Na phases relative to fcc (ΔH). The fcc \rightarrow $cI16 \rightarrow$ $tI19 \rightarrow$ $hP4$ ($oP8$) transitions are calculated at 121, 147, and 268 GPa, respectively. Besides the experimentally observed Na structures (fcc [43], $cI16$ [4,5], $oP8$ [4], $tI19$ [4], and $hP4$ [6]), seven novel phases found in the evolutionary searches (five shown in the inset) were chosen for further analysis. (b) The Gibbs free energy of $P6_3/m$ Na relative to $hP4$ (ΔG) as a function of temperature T and pressure P . A negative ΔG (blue region) indicates that $P6_3/m$ is more stable than $hP4$. The green dots with black arrows highlight the critical conditions where $P6_3/m$ becomes preferred at low (150 K and 200 GPa) and high (1900 K and 350 GPa) temperatures. (c) ΔG of various Na phases relative to $hP4$ at 300 GPa. $P6_3/m$ becomes the most stable phase above 1240 K.

To search for potential candidate structures that could be stable or metastable at the aforementioned conditions, we performed extensive structure searches using the XTALOPT [28,29] evolutionary algorithm coupled with DFT calculations (see Supplemental Material [42] for more detailed information). Besides the previously reported sodium structures, seven additional dynamically stable (Sec. S5 of the Supplemental Material [42]) low-enthalpy phases were found in the evolutionary runs, consistent with the results of the ramp-compression experiments that hinted of a complex free-energy landscape in sodium at these conditions. These $R3$, $P2_1/m$, $C2/m$, $P6_3/m$, $P\bar{3}m1$, $Fmm2$, and $P\bar{6}2m$ symmetry (Table S2) polymorphs were therefore singled out for further analysis.

Figure 1(a) illustrates that our calculated cold phase-transition sequences and corresponding pressures are in good agreement with experiment and previous calculations [6]. These static lattice enthalpies, however, do not include zero-point or finite temperature effects, which have been shown to play an important role in the phase stability of Na [4]. Therefore, the thermodynamic stability of the structural candidates was studied by calculating their Gibbs free energies within the quasiharmonic approximation (Sec. S6 of the Supplemental Material [42]). The effects of temperature on phase stability, especially at extreme pressures, are not often addressed

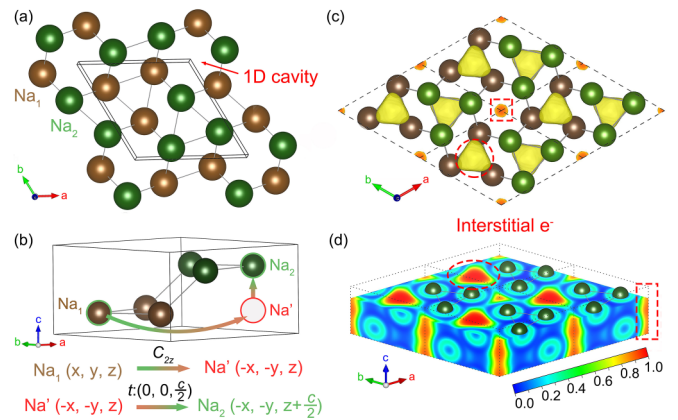


FIG. 2. (a) The crystal structure of $P6_3/m$ Na highlighting the 1D cavity along the c axis by a red arrow. The green and brown atoms indicate the Na atoms lying in two different ab planes. (b) Side view of the unit cell of $P6_3/m$ Na. An illustration of a nonsymmorphic symmetry operation, S_{2z} , that includes a C_{2z} rotation and $t = (0, 0, \frac{c}{2})$ translation is indicated. (c) Valence electron localization function (ELF) with isosurface value of 0.80. (d) Contour map of the ELF, where the red and blue colors refer to the highest (1.0) and the lowest (0.0) values. The dashed red circles (rectangles) in panels (c) and (d) show that the anionic electrons are located within 0D cages (1D honeycomb channels).

theoretically because of the expense associated with performing these calculations. However, recent high-profile publications on the dynamic compression of water [44], magnesium [45], diamond [46], and now sodium [7] find that the structures calculated to be most stable at 0 K are not necessarily those that are observed at high temperatures. Because the phases created usually cannot be identified by experimental methods alone, computational protocols must be developed to propose viable candidates.

Comparison of the free energies showed that all of the seven newly discovered structures were preferred over Na $hP4$ (Sec. S6 of the Supplemental Material [42]) at characteristic pressure and temperature regimes, hinting of the possibility of rich structural polymorphism. In particular, we note a $P6_3/m$ symmetry phase that was computed to be more stable than Na $hP4$ at 200 GPa (350 GPa) above 150 K (1900 K) [Fig. 1(b)]. In contrast, the relative enthalpies alone suggest that at 300 GPa $P6_3/m$ Na is 62 meV/atom less stable than $hP4$ Na, highlighting the importance of the finite-temperature effects on the lattice energies. The absence of imaginary frequencies in the phonon spectra confirmed the dynamic stability of $P6_3/m$ Na from 150 to 350 GPa. In fact, out of all of the Na phases considered $P6_3/m$ was computed to possess the lowest Gibbs free energy between 250 GPa (above 710 K) and 350 GPa (above 1900 K). At 400 GPa Na $hP4$ was the most stable structure to at least 3500 K (see Fig. S8 of the Supplemental Material [42]), in agreement with experimental diffraction data that could be attributed to this phase at 409 ± 15 GPa [7].

Because the $P6_3/m$ Na phase is the most stable at high temperatures and intermediate pressures, let us take a closer look at its geometrical and electronic peculiarities. This structure, illustrated in Fig. 2(a), belongs to a nonsymmorphic space

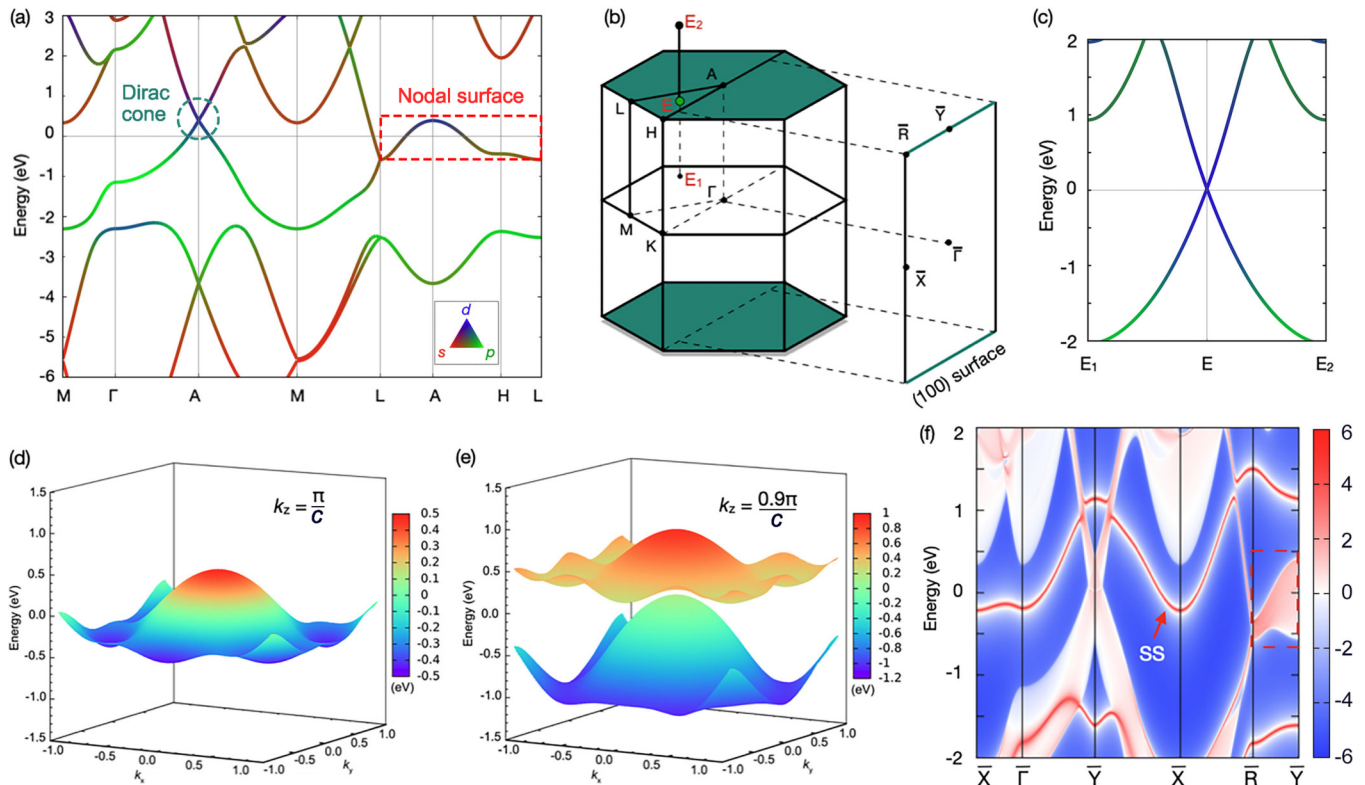


FIG. 3. (a) Band structure of $P6_3/m$ Na at 350 GPa, with the band coloring indicating the orbital character (red, green, blue Na s , p , d). (b) 3D BZ of $P6_3/m$ Na and its projection onto a 2D BZ on the (100) surface. High-symmetry and arbitrary (E_1 - E - E_2) points are labeled. (c) Band structure along the arbitrary E_1 - E - E_2 line that lies perpendicular to the $k_z = \pi/c$ plane at the arbitrary E point that is located in the plane, as shown in panel (b). (d), (e) The 3D plot of the valence and conduction bands in the $k_z = \pi/c$ and $k_z = 0.9\pi/c$ plane, respectively. The color represents the energy of the bands relative to E_F . The bands are relatively flat and fourfold degenerate in the $k_z = \pi/c$ plane (neglecting SOC), which is the nodal surface. The bands split in the $k_z = 0.9\pi/c$ plane. (f) Band structure projected on the (100) surface, with the surface state (SS) denoted by a red arrow. The bands enclosed by the red dashed rectangle highlight the projection of the topological nodal surface.

group (No. 176) lacking mirror, and other roto-inversion symmetries. However, it possesses a nonsymmorphic symmetry [Fig. 2(b)] generated by a twofold screw rotation along the c axis $S_{2z} : (x, y, z) \rightarrow (-x, -y, z + c/2)$. This same symmetry operation has been reported to provide protection for topological nodal surface states in various crystalline materials that are stable at ambient conditions [47–49]. Plots of the electron localization function [ELF, Fig. 2(c) and 2(d)] reveal that $P6_3/m$ Na is an electride where paired electrons are localized in 1D honeycomb channels that run along the c axis, key for the semimetallic nature of this phase. Further electron density is localized within 0D electron blobs centered on the interstitial regions within the Na_9 tricapped trigonal prisms. Previous computational studies have shown that similar 1D chains of localized electrons are a striking feature of the ELF plot of $P6_3/m$ symmetry Ba_3CrN_3 (Fig. S24 of the Supplemental Material [42]) and Sr_3CrN_3 —known inorganic topological electrides stable at ambient conditions, which were predicted to possess anomalous Dirac plasmons with unique properties such as a long lifetime [49].

The band structure of $P6_3/m$ Na at 350 GPa [PBE functional Fig. 3(a), and HSE06 functional in Fig. S18 of the Supplemental Material [42]] is characteristic of a semimetal. The dispersion is large along the metallic k_z direction, confirming the 1D nature of localized electrons within the

honeycomb channels. A plot of the charge density of the $P6_3/m$ phase in a 1 eV energy window around E_F (Fig. S17 of the Supplemental Material [42]) shows that the degenerate bands of the nodal surface are mostly a result of these 1D-localized anionic electrons, in agreement with recent theoretical studies of Ba_3CrN_3 and Sr_3CrN_3 [47,49]. In comparison, the dispersion along the $k_z = 0$ plane with insulating character is relatively small, due to the localized nature of the charge density within this plane. The valence and conduction bands meet in the vicinity of E_F and form a band crossing at the high-symmetry A point. Along the L - A - H - L path, which lies in the $k_z = \pi/c$ plane, the bands stick together and are fourfold degenerate. Plotting the band structure along an arbitrary line, E_1 - E - E_2 , which is perpendicular to the $k_z = \pi/c$ plane at the E point located in this plane [Fig. 3(b)], illustrates that the degeneracy remains at this point. This is seen clearly at E where the Dirac nodal point lies [Fig. 3(c)], suggesting that the degeneracy may be present throughout the whole $k_z = \pi/c$ plane. Plotting the three-dimensional (3D) band structure near E_F while varying k_x and k_y , but keeping $k_z = \pi/c$ fixed [Fig. 3(d)] confirms our conjecture that the valence and conduction bands are degenerate within this plane. Therefore, the continuous nodal points form a Dirac nodal surface throughout the whole BZ. A plot of the valence and conduction band energies at $k_z = 0.9\pi/c$ illustrates that

the degeneracy is broken [Fig. 3(e)]. Because of the small but non-negligible coupling between the 1D anionic electrons within the honeycomb channels, the Dirac nodal surface is not entirely flat, in line with previous results for Ba_3CrN_3 [49]. Within the nodal surface only a ring around the A point is situated exactly at E_F . Thus, the electronic properties of $P6_3/m$ Na may be similar to those of nodal ring materials, such as Li at intermediate pressures [22,23]. Calculations including spin-orbit coupling (SOC) illustrate that the band splitting is negligible for these loosely bound anionic electrons (Fig. S16 of the Supplemental Material [42]), as expected.

The presence of the Dirac nodal surface in $P6_3/m$ is dictated by the nonsymmorphic symmetry S_{2z} . The protection mechanism was previously described in Refs. [47–49], and measured [50,51] in a variety of 3D topological materials. $P6_3/m$ Na possesses time-reversal symmetry ($T^2 = 1$), and the TS_{2z} operation satisfies $(TS_{2z})^2 = e^{-ik_z}$. As a result, any point on the $k_z = \pi/c$ plane is invariant such that $(TS_{2z})^2 = -1$, ensuring that a twofold Kramers degeneracy arises at every point on the plane, which is therefore characterized by a topological nodal surface [47,48].

The band structure projected on the (100) surface [Fig. 3(f)] illustrates that a surface state band, which does not belong to the projected bulk band structure, crosses E_F . Such a metallic surface state is also detected in the band structure projected on the (-110) surface (Fig. S15 of the Supplemental Material [42]). Meanwhile, the projection of the Dirac nodal surface is observed along the $\bar{R}-\bar{Y}$ path. The presence of metallic surface states illustrates the topological features of the high-pressure, high-temperature $P6_3/m$ Na phase.

Could the experimental XRD pattern obtained at intermediate pressures and high temperatures in Ref. [7] be indexed for this low-enthalpy $P6_3/m$ Na phase? As previously noted, the observed peaks could not be indexed by the $hP4$ phase alone, and the proposed $cI16$ and $R\bar{3}m$ phases turned out to be dynamically and thermally unstable at these conditions. To study this further, the $P6_3/m$ lattice parameters were refined using a least squares optimization to match its XRD pattern with the experimental XRD pattern. The refinement considered only the observed diffraction angle 2θ 's of the peaks, but not their intensities. Figure 4 shows a comparison of the XRD pattern calculated for this refined lattice using the wavelength characteristic of He- α Cu radiation (8.37 keV) with the experimental lineouts along 2θ at ≈ 260 GPa and ≈ 315 GPa from Ref. [7]. First principles molecular-dynamics simulations revealed that the refined $P6_3/m$ structure is thermally stable at 260 GPa and 1500 K, as well as at 315 GPa and 2000 K (Sec. S7 of the Supplemental Material [42]).

Examination of Fig. 4 shows that the diffraction pattern from $P6_3/m$ Na contains features that are consistent with the experimental data at both 260 and 315 GPa; however, the experimental pattern cannot be described entirely by the $P6_3/m$ phase. A key difference is the absence of peaks at $\approx 35^\circ$ and $\approx 36^\circ$, respectively, for the $P6_3/m$ structure. Such low-angle peaks are present in the XRD patterns simulated for Na $hP4$. Moreover, the refined lattice parameters yield a volume that is smaller than that of the other phases (Fig. S2 of the Supplemental Material [42]), implying that a large density jump occurs with increasing pressure. Thus, the $P6_3/m$ structure reported here cannot, on its own, explain the experimental

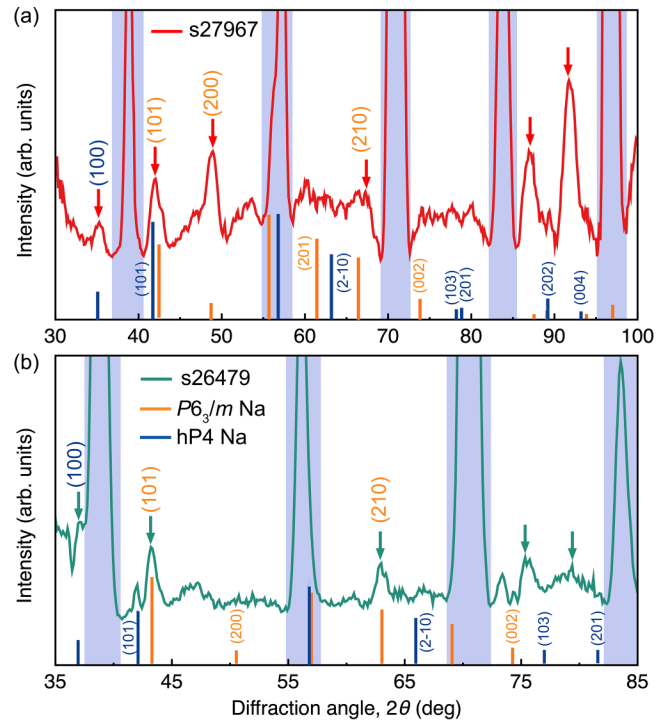


FIG. 4. Simulated XRD patterns ($\lambda = 1.4813 \text{ \AA}$) and experimental lineouts along 2θ [7] of Na under pressure. The (a) red [(b) green] curves depict the experimental patterns from shot 27697 (26479) at 261 ± 11 GPa (315 ± 11 GPa). The vertical ticks correspond to expected positions and intensities of XRD peaks for the refined $P6_3/m$ (yellow) and $hP4$ (blue) symmetry Na structures at 260 GPa (315 GPa). The Na atoms in the $P6_3/m$ structure lie on the $6h$ Wyckoff site (0.110, 0.734, 0.250) with refined lattice parameters of $a = b = 4.132 \text{ \AA}$, and $c = 2.472 \text{ \AA}$ ($a = b = 4.015 \text{ \AA}$, and $c = 2.450 \text{ \AA}$). The $hP4$ structure contains Na atoms on the $2a$ (0, 0, 0) and $2c$ (1/3, 2/3, 3/4) Wyckoff sites with lattice parameters of $a = b = 2.845 \text{ \AA}$, and $c = 4.062 \text{ \AA}$ ($a = b = 2.705 \text{ \AA}$, and $c = 4.128 \text{ \AA}$, refined). The shaded vertical regions provide the positions of the experimental pinhole calibration peaks.

data. Further experimental investigations of phase space and computations considering anharmonic and quantum nuclear effects are required.

Besides the topological $P6_3/m$ phase, six new phases of high-pressure sodium, $P2_1/m$ (< 300 GPa), $R3$ (> 300 GPa), $C2/m$ (> 300 GPa), $P\bar{3}m1$ (> 250 GPa), $Fmm2$ (> 175 GPa), and $P\bar{6}2m$ (> 150 GPa) were computed as dynamically stable at the pressures given in the brackets (Fig. S6 of the Supplemental Material [42]). From these, three were semiconductors or insulators ($P2_1/m$, $C2/m$, and $R3$) and three were metals ($P\bar{3}m1$, $P\bar{6}2m$, and $Fmm2$) (Figs. S20–S21 of the Supplemental Material [42]). ELF calculations (Sec. S10 of the Supplemental Material [42]) showed that all of these phases are electriles with charge localized in 0D blobs or 1D features. Just like $P6_3/m$, the interstitial electron density in the $Fmm2$ phase was confined to 0D and 1D spatial regions. However, due to the lack of nonsymmorphic symmetry, the $Fmm2$ phase was calculated to be a conventional metal without any topological features. The same is true for $P\bar{3}m1$ and $P\bar{6}2m$, while $P2_1/m$, $C2/m$, and $R3$ were confirmed to be trivial insulators.

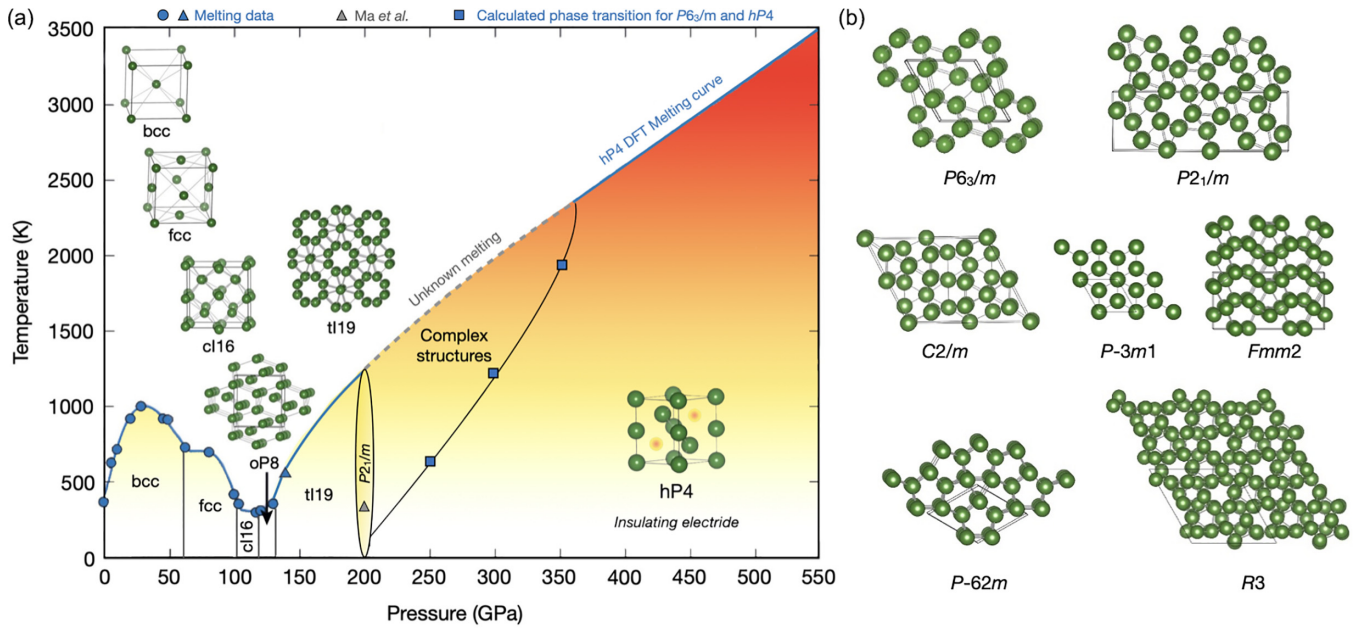


FIG. 5. (a) The pressure-temperature phase diagram of Na along with the known bcc, fcc, $oP8$, $cI16$, $tI19$, and $hP4$ crystal structures from previous studies [4,6,7]. We schematically illustrate the P - T region where the predicted $P2_1/m$ phase is likely to be the most stable, and label the region where, in addition to $hP4$, the seven structures shown in the right panel are predicted to possess low free energies. The gray triangle denotes the P - T conditions where the $hP4$ phase was made [6]. The melting curve data from Refs. [3] and [13] are shown (blue circles and triangle) along with a Kechin [54] fit to DFT calculations for the melting curve for the $hP4$ phase [14], and the gray dashed line depicts the unknown melting curve for the complex structures. (b) The newly predicted $P6_3/m$, $P2_1/m$, $C2/m$, $P\bar{3}m1$, $Fmm2$, $P\bar{6}2m$, and $R3$ phases.

In our calculations the incommensurate $tI19$ phase was modeled with a 58 atom unit cell. At 200 GPa and 0 K it was the ground state with the $P2_1/m$ ($\Delta H = 25$ meV/atom) and $hP4$ ($\Delta H = 29$ meV/atom) phases being metastable. However, the large unit cell made calculations of the free energy of the $tI19$ model prohibitively expensive. Without it, $P2_1/m$ Na was found to be preferred over $hP4$ at 200 GPa in the whole temperature range studied, see Fig. S8(a) of the Supplemental Material [42], suggesting that all three of these structures are competitive at this pressure. Therefore, experiments that attempt to create $P2_1/m$ Na are suggested. To facilitate the comparison of theory and experiment the simulated XRD pattern of all of these phases is provided in Fig. S26 of the Supplemental Material [42]. The $C2/m$, $P\bar{3}m1$, $Fmm2$, $P\bar{6}2m$, and $R3$ Na phases were metastable and did not possess the lowest free energies at any P - T region considered in this work.

Figure 5 presents a schematic phase diagram for sodium, combining experimental static [4,6] and dynamic compression [7] data, as well as measured and predicted melting curve data [3,13,14]. Besides the experimentally verified bcc, fcc, $oP8$, $cI16$, $tI19$, and $hP4$ phases, we highlight a region where our quasiharmonic calculations found $P2_1/m$ to be the free-energy minimum, as described above. The region where $P6_3/m$ Na was the most stable—but where numerous phases may be experimentally accessible due to their small range of free energies—is labeled as “complex structures” in this plot. Between ≈ 200 – 350 GPa it may be necessary to revise the calculated melting curve [14], as it was obtained assuming the $hP4$ structure. Our study suggests that the structural diversity discovered near the minimum of the melting curve of sodium at room temperature and 140 GPa [4], extends to >300 GPa and thousands of degrees K.

IV. CONCLUSION

In summary, *ab initio* evolutionary structure searches coupled with quasiharmonic calculations illustrate that a novel $P6_3/m$ symmetry Na phase becomes preferred over the known Na $hP4$ structure at 250 GPa (350 GPa) above 710 K (1900 K). Importantly, seven sodium polymorphs were found to be dynamically stable within this region of the phase diagram. Their 0 K free energies differed by up to 200 meV/atom, with finite-temperature effects lowering this difference to between 40–90 meV/atom. This complex polymorphism could explain why, in this pressure and temperature regime, no single structure is fully consistent with the XRD data obtained in laser-driven ramp-compression experiments at 260 and 315 GPa [7] (see Fig. S25 of the Supplemental Material [42]). The pressure and temperature gradients present in the sample may lead to the coexistence of a number of phases. Above 400 GPa Na $hP4$ is predicted to be the ground-state structure independent of temperature, in agreement with the experimental observations.

$P6_3/m$ Na is a semimetallic electride owing to 1D chains of interstitial electrons that run along honeycomb channels, and electron blobs localized in Na_9 cages. Electronic structure calculations reveal that $P6_3/m$ Na possesses a Dirac nodal surface state that is topologically protected by the non-symmorphic symmetry S_{2z} , suggesting it may exhibit unique properties such as anomalous Dirac plasmons predicted to be present in other 1D topological electrides [49]. We hope this study stimulates further work of Na’s structural complexity, topological properties, and core-electron chemistry under extreme conditions of pressure and temperature found within the cores of Earth-like planets and mantles of superearths.

ACKNOWLEDGMENTS

We are grateful to G. W. Collins, J. Eggert, R. J. Hemley, S. X. Hu, S. Racioppi, and S. Zhang for useful discussions. This material is based upon work supported by the Department of Energy National Nuclear Security Administration under Award No. DE-NA0003856, the University of Rochester, and the New York State Energy Research and Development Authority. K.P.H. acknowledges the Chicago/DOE Alliance Center under Cooperative Agreement Grant No. DE-

NA0003975. This material is based upon work supported by the U.S. Department of Energy, Office of Science, Fusion Energy Sciences funding the award entitled *High Energy Density Quantum Matter* under Award No. DE-SC0020340. Partial funding for this research is provided by the Center for Matter at Atomic Pressures (CMAP), a National Science Foundation (NSF) Physics Frontiers Center, under Award No. PHY-2020249. Computations were carried out at the Center for Computational Research at the University at Buffalo [52].

-
- [1] B. Rousseau, Y. Xie, Y. Ma, and A. Bergara, *Eur. Phys. J. B* **81**, 1 (2011).
- [2] S. F. Elatresh, M. T. Hossain, T. Bhowmick, A. D. Grockowiak, W. Cai, W. A. Coniglio, S. W. Tozer, N. W. Ashcroft, S. A. Bonev, S. Deemyad, and R. Hoffmann, *Phys. Rev. B* **101**, 220103(R) (2020).
- [3] E. Gregoryanz, O. Degtyareva, M. Somayazulu, R. J. Hemley, and H.-k. Mao, *Phys. Rev. Lett.* **94**, 185502 (2005).
- [4] E. Gregoryanz, L. F. Lundegaard, M. I. McMahon, C. Guillaume, R. J. Nelmes, and M. Mezouar, *Science* **320**, 1054 (2008).
- [5] M. McMahon, E. Gregoryanz, L. Lundegaard, I. Loa, C. Guillaume, R. Nelmes, A. Kleppe, M. Amboage, H. Wilhelm, and A. Jephcoat, *Proc. Natl. Acad. Sci. USA* **104**, 17297 (2007).
- [6] Y. Ma, M. Eremets, A. R. Oganov, Y. Xie, I. Trojan, S. Medvedev, A. O. Lyakhov, M. Valle, and V. Prakapenka, *Nature (London)* **458**, 182 (2009).
- [7] D. N. Polsin, A. Lazicki, X. Gong, S. J. Burns, F. Coppari, L. E. Hansen, B. J. Henderson, M. F. Huff, M. I. McMahon, M. Millot, R. Paul, R. F. Smith, J. H. Eggert, G. W. Collins, and J. R. Rygg, *Nat. Commun.* **13**, 2534 (2022).
- [8] J. B. Neaton and N. W. Ashcroft, *Phys. Rev. Lett.* **86**, 2830 (2001).
- [9] B. Rousseau and N. W. Ashcroft, *Phys. Rev. Lett.* **101**, 046407 (2008).
- [10] M.-S. Miao and R. Hoffmann, *Acc. Chem. Res.* **47**, 1311 (2014).
- [11] M. Miao, Y. Sun, E. Zurek, and H. Lin, *Nat. Rev. Chem.* **4**, 508 (2020).
- [12] M. Gatti, I. V. Tokatly, and A. Rubio, *Phys. Rev. Lett.* **104**, 216404 (2010).
- [13] M. Marqués, M. Santoro, C. L. Guillaume, F. A. Gorelli, J. Contreras-García, R. T. Howie, A. F. Goncharov, and E. Gregoryanz, *Phys. Rev. B* **83**, 184106 (2011).
- [14] R. Paul, S. X. Hu, V. V. Karasiev, S. A. Bonev, and D. N. Polsin, *Phys. Rev. B* **102**, 094103 (2020).
- [15] J. Y. Raty, E. Schwegler, and S. A. Bonev, *Nature (London)* **449**, 448 (2007).
- [16] Y. Li, Y. Wang, C. J. Pickard, R. J. Needs, Y. Wang, and Y. Ma, *Phys. Rev. Lett.* **114**, 125501 (2015).
- [17] L. M. Schoop, F. Pielnhofer, and B. V. Lotsch, *Chem. Mater.* **30**, 3155 (2018).
- [18] N. Kumar, S. N. Guin, K. Manna, C. Shekhar, and C. Felser, *Chem. Rev. (Washington, DC, US)* **121**, 2780 (2021).
- [19] I. I. Naumov and R. J. Hemley, *Phys. Rev. Lett.* **117**, 206403 (2016).
- [20] I. I. Naumov and R. J. Hemley, *Phys. Rev. B* **96**, 035421 (2017).
- [21] J. Hooper and E. Zurek, *ChemPlusChem* **77**, 969 (2012).
- [22] S. A. Mack, S. M. Griffin, and J. B. Neaton, *Proc. Natl. Acad. Sci. USA* **116**, 9197 (2019).
- [23] S. F. Elatresh, Z. Zhou, N. W. Ashcroft, S. A. Bonev, J. Feng, and R. Hoffmann, *Phys. Rev. Mater.* **3**, 044203 (2019).
- [24] K. S. Novoselov, A. K. Geim, S. V. Morozov, D.-e. Jiang, Y. Zhang, S. V. Dubonos, I. V. Grigorieva, and A. A. Firsov, *Science* **306**, 666 (2004).
- [25] T. Liang, Q. Gibson, M. N. Ali, M. Liu, R. Cava, and N. Ong, *Nat. Mater.* **14**, 280 (2015).
- [26] S. Guan, Z.-M. Yu, Y. Liu, G.-B. Liu, L. Dong, Y. Lu, Y. Yao, and S. A. Yang, *npj Quantum Mater.* **2**, 23 (2017).
- [27] B. Q. Lv, T. Qian, and H. Ding, *Rev. Mod. Phys.* **93**, 025002 (2021).
- [28] D. C. Lonie and E. Zurek, *Comput. Phys. Commun.* **182**, 372 (2011).
- [29] Z. Falls, P. Avery, X. Wang, K. P. Hilleke, and E. Zurek, *J. Phys. Chem. C* **125**, 1601 (2021).
- [30] P. Avery, C. Toher, S. Curtarolo, and E. Zurek, *Comput. Phys. Commun.* **237**, 274 (2019).
- [31] G. Kresse and J. Furthmüller, *Phys. Rev. B* **54**, 11169 (1996).
- [32] G. Kresse and J. Furthmüller, *Comput. Mater. Sci.* **6**, 15 (1996).
- [33] J. P. Perdew, K. Burke, and M. Ernzerhof, *Phys. Rev. Lett.* **77**, 3865 (1996).
- [34] H. J. Monkhorst and J. D. Pack, *Phys. Rev. B* **13**, 5188 (1976).
- [35] S. Baroni, S. De Gironcoli, A. Dal Corso, and P. Giannozzi, *Rev. Mod. Phys.* **73**, 515 (2001).
- [36] X. Gonze, *Phys. Rev. A* **52**, 1096 (1995).
- [37] A. Togo, F. Oba, and I. Tanaka, *Phys. Rev. B* **78**, 134106 (2008).
- [38] A. Carreras, A. Togo, and I. Tanaka, *Comput. Phys. Commun.* **221**, 221 (2017).
- [39] A. A. Mostofi, J. R. Yates, G. Pizzi, Y.-S. Lee, I. Souza, D. Vanderbilt, and N. Marzari, *Comput. Phys. Commun.* **185**, 2309 (2014).
- [40] Q. Wu, S. Zhang, H.-F. Song, M. Troyer, and A. A. Soluyanov, *Comput. Phys. Commun.* **224**, 405 (2018).
- [41] Y. He, Y. Jiang, T. Zhang, H. Huang, C. Fang, and Z. Jin, *Chin. Phys. B* **28**, 087102 (2019).
- [42] See Supplemental Material at <http://link.aps.org/supplemental/10.1103/PhysRevB.107.184101> for computational details, structural parameters, as well as extra analysis and plots related to the electronic structure, phonon dispersions, thermodynamic stability at finite temperatures, molecular dynamics simulations, electron localization function, topological properties, as well as text related to Refs. [53–60].

- [43] M. Hanfland, I. Loa, and K. Syassen, *Phys. Rev. B* **65**, 184109 (2002).
- [44] M. Millot, S. Hamel, J. R. Rygg, P. M. Celliers, G. W. Collins, F. Coppari, D. E. Fratanduono, R. Jeanloz, D. C. Swift, and J. H. Eggert, *Nat. Phys.* **14**, 297 (2018).
- [45] M. Gorman, S. Elatresh, A. Lazicki, M. Cormier, S. Bonev, D. McGonegle, R. Briggs, A. Coleman, S. Rothman, L. Peacock *et al.*, *Nat. Phys.* **18**, 1307 (2022).
- [46] A. Lazicki, D. McGonegle, J. Rygg, D. Braun, D. Swift, M. Gorman, R. Smith, P. Heighway, A. Higginbotham, M. J. Suggit *et al.*, *Nature (London)* **589**, 532 (2021).
- [47] Q.-F. Liang, J. Zhou, R. Yu, Z. Wang, and H. Weng, *Phys. Rev. B* **93**, 085427 (2016).
- [48] W. Wu, Y. Liu, S. Li, C. Zhong, Z.-M. Yu, X.-L. Sheng, Y. X. Zhao, and S. A. Yang, *Phys. Rev. B* **97**, 115125 (2018).
- [49] J. Wang, X. Sui, S. Gao, W. Duan, F. Liu, and B. Huang, *Phys. Rev. Lett.* **123**, 206402 (2019).
- [50] Y. Yang, J.-p. Xia, H.-x. Sun, Y. Ge, D. Jia, S.-q. Yuan, S. A. Yang, Y. Chong, and B. Zhang, *Nat. Commun.* **10**, 5185 (2019).
- [51] M. Xiao, L. Ye, C. Qiu, H. He, Z. Liu, and S. Fan, *Sci. Adv.* **6**, eaav2360 (2020).
- [52] <http://hdl.handle.net/10477/79221>.
- [53] D. C. Lonie and E. Zurek, *Comput. Phys. Commun.* **183**, 690 (2012).
- [54] V. V. Kechin, *Phys. Rev. B* **65**, 052102 (2001).
- [55] J. Heyd, G. E. Scuseria, and M. Ernzerhof, *J. Chem. Phys.* **118**, 8207 (2003).
- [56] F. Birch, *J. Geophys. Res.* **57**, 227 (1952).
- [57] P. Blaha, K. Schwarz, P. Sorantin, and S. Trickey, *Comput. Phys. Commun.* **59**, 399 (1990).
- [58] P. Avery and E. Zurek, *Comput. Phys. Commun.* **213**, 208 (2017).
- [59] G. Kresse and D. Joubert, *Phys. Rev. B* **59**, 1758 (1999).
- [60] P. E. Blöchl, *Phys. Rev. B* **50**, 17953 (1994).